ORIGINAL ARTICLE

DOI: 10.4274/jcrpe.galenos.2025.2025-1-18

J Clin Res Pediatr Endocrinol 2025;17(4):436-448

Diagnostic Utility of Next-Generation Sequencing-based CNV Analysis in Eleven Patients with Peters-Plus Syndrome: A Single-Center Experience

Akçahan Akalın[1], Enise Avcı Durmuşalioğlu[2], Şervan Özalkak[3], Ruken Yıldırım[3], Veysel Öz[4], Edip Ünal[5], Leyla Hazar[6], Türkan Turkut Tan[2], Yusuf Can Doğan[2], Tahir Atik[2], Özgür Çoğulu[2], Esra Işık[2]

[1]Diyarbakır Children's Hospital, Clinic of Pediatric Genetics, Diyarbakır, Türkiye
[2]Ege University Faculty of Medicine, Department of Pediatrics, Division of Pediatric Genetics, İzmir, Türkiye
[3]Diyarbakır Children's Hospital, Clinic of Pediatric Endocrinology, Diyarbakır, Türkiye
[4]Diyarbakır Children's Hospital, Clinic of Pediatric Neurology, Diyarbakır, Türkiye
[5]Dicle University Faculty of Medicine, Department of Pediatric Endocrinology, Diyarbakır, Türkiye
[6]Dicle University Faculty of Medicine, Department of Ophthalmology, Diyarbakır, Türkiye

What is already known on this topic?

Peters-Plus syndrome (PTRPLS) is a rare genetic condition caused by biallelic pathogenic variants in the ß 1,3-glucosyltransferase gene (*B3GLCT*). Affected individuals exhibited anterior eye-chamber defects, disproportionate short stature, facial dysmorphism and developmental delay.

What this study adds?

To the best of our knowledge, this is the first report demonstrating that exonic deletions can contribute to the pathogenesis of PTRPLS. We report the smallest homozygous deletion identified on chromosome 13q12, encompassing the fifteenth exonof the *B3GLCT* gene in PTRPLS patients.

Abstract

Objective: Peters-Plus syndrome (PTRPLS) is an autosomal recessive congenital disorder of glycosylation caused by biallelic pathogenic variants in the ß 1,3-glucosyltransferase gene (*B3GLCT*). To date, homozygous or compound heterozygous splicing, truncating, missense variants, and whole gene deletions have been reported in the *B3GLCT* gene. Our aim was to investigate the role of small copy number variations (CNVs) in this condition alongside the clinical features of the patients.

Methods: The study included eleven patients from six consanguineous families originating from the same village. Clinical exome sequencing-based CNV analysis was employed across all probands to ascertain the genetic background.

Results: Using GATK-gCNV, we identified a homozygous deletion on chromosome 13q12.3, encompassing the fifteenth exon of the *B3GLCT* gene. The median age at admission was 2.74 years, ranging from 2 months to 41 years. The mean standard deviation scores for height and weight at admission were -4.4 ± 0.9 and -3.8 ± 1.8, respectively. Ophthalmological abnormalities included corneal haze, anterior synechiae, unilateral leucoma, corneal-lenticular adhesion, glaucoma, and severe visual loss. Patients under the age of five years exhibited global developmental delay, while those older than five years demonstrated varying degrees of intellectual disability, with two exceptions exhibiting normal cognitive function.

Cite this article as: Akalın A, Avcı Durmuşalioğlu E, Özalkak Ş, Yıldırım R, Öz V, Ünal E, Hazar L, Turkut Tan T, Doğan YC, Atik T, Çoğulu Ö, Işık E. Diagnostic utility of next-generation sequencing-based CNV analysis in eleven patients with Peters-Plus syndrome: a single-center experience. J Clin Res Pediatr Endocrinol. 2025;17(4):436-448

Address for Correspondence: Enise Avcı Durmuşalioğlu MD, Ege University Faculty of Medicine, Department of Pediatrics, Division of Pediatric Genetics, İzmir, Türkiye
E-mail: eniseavci.ea@gmail.com **ORCID:** orcid.org/0000-0002-0582-8881

Conflict of interest: None declared
Received: 28.01.2025
Accepted: 27.03.2025
Epub: 11.04.2025
Publication date: 11.12.2025

Conclusion: Our findings highlight an important role for Next-Generation Sequencing (NGS)-based CNV analysis in improving the diagnostic accuracy in PTRPLS. CNVs represent a significant form of genomic variation and should be systematically considered in genetically unresolved Mendelian disorders. Integrating CNV detection algorithms into routine NGS diagnostic workflows has the potential to enhance the identification of pathogenic changes, ultimately facilitating a more comprehensive molecular diagnosis for affected individuals.

Keywords: Peters-Plus syndrome, copy number variation, next-generation sequencing, Mendelian disorders

Introduction

Peters-Plus syndrome (PTRPLS; OMIM #261540) is a rare autosomal recessive congenital disorder of glycosylation caused by mutations in the ß 1,3-glucosyltransferase gene (*B3GLCT*). PTRPLS typically presents with a spectrum of clinical features encompassing ocular defects, disproportionate short stature, clefting and developmental delay (1). Ocular manifestations primarily involve the anterior chamber, with the hallmark being Peters anomaly characterized by corneal clouding and adhesions between the iris, lens, and cornea (2,3,4,5). The term "Peters' Plus syndrome" was introduced in 1984 by Dutch ophthalmologist van Schooneveld et al. (6), who described 11 patients with anterior eye chamber defects, clefting, short limb dwarfism, and developmental delay. Decades later, the molecular etiology was elucidated using genome-wide 1-Mb resolution array-based comparative genomic hybridization and Sanger sequencing, which identified a ~1.5-Mb interstitial deletion on chromosome 13q12.3q13.1 encompassing the causative gene *B3GLCT*, along with the common c.660+1G>A variant on the other allele (1). To date, splicing, truncating, missense variants, and whole gene deletions have been reported in *B3GLCT* (7). *B3GLCT* plays a crucial role in the modification of proteins during glycosylation. O-fucose is added to cysteine-rich domains known as thrombospondin type 1 repeats (TSRs) by protein O-fucosyltransferase 2 (POFUT2) and is subsequently elongated with glucose by B3GLCT (8). Previous studies have indicated that O-linked fucose is crucial for the proper folding and secretion of POFUT2-modified proteins and that the extension of the disaccharide by B3GLCT is vital for only a subset of these targets. Patients with PTRPLS are affected by the reduced function of specific POFUT2/B3GLCT targets, resulting from the loss of B3GLCT activity.

In the present study, the aim was to evaluate eleven patients diagnosed with PTRPLS using Next-Generation Sequencing (NGS)-based copy number variation (CNV) analysis and to highlight novel molecular approaches that may elucidate the genetic background of rare Mendelian disorders. Traditional techniques, such as microarrays and multiplex ligation-dependent probe amplification (MLPA), have been commonly used for CNV detection. However, the introduction of NGS-based CNV analysis has revolutionized the field with its efficiency and cost-effectiveness (9).

Methods

Patients and Samples

The study received approval from the Non-invasive Clinical Research Ethical Committee of University of Health Sciences Türkiye, Diyarbakır Gazi Yaşargil Training and Research Hospital (approval number: 46, date: 10.05.2024). The molecular genetic analysis, including NGS-based CNV analysis, was performed as previously described (10,11,12,13,14). Written informed consent was obtained from their legal parents or guardians, including permission to publish clinical information and photographs of the children. One ophthalmologist and one pediatric genetic specialist evaluated all cases. After a thorough physical examination, dysmorphic features and anthropometric measurements were noted, and standard deviation scores (SDS) were calculated and recorded. SDS was calculated using a national pediatric calculator following national standards (https://www.ceddcozum.com). Demographic features, family history, and clinical and radiographic findings were all obtained from retrospective data. Ophthalmologic examinations were conducted using the following methods: Anterior segment examination was performed with slit-lamp bimicroscopy. Intraocular pressure was measured using an I-care tonometer (I-care Finland Oy, Vantaa, Finland). Pupil dilation was achieved with 1% tropicamide, followed by a detailed fundus examination. For patients whose fundus could not be visualized due to anterior segment pathology, retinal evaluation was performed using B-scan ultrasonography. The clinical diagnosis of PTRPLS was established based on dysmorphic features and molecular genetic results.

Genetic Analysis

Sample Collection: Peripheral blood samples were collected from patients and their family members, and genomic DNA was extracted using the MagNA Pure 96 DNA and Viral NA Small Volume Kit (Roche Diagnostics GmbH, Mannheim, Germany).

Sample Preparation: Clinical exome sequencing (CES) was performed using the HyperCap Design Share Inherited Disease Panel (covering 4,125 genes; Roche Sequencing Solutions, Pleasanton, CA, USA) for target enrichment, and libraries were prepared with the KAPA HyperExome kit (Roche Sequencing Solutions, Pleasanton, CA, USA). Samples were prepared following the respective kit protocols, which involved capturing exonic regions of interest using targeted probes.

Sequencing: The prepared libraries were sequenced on the DNBSEQ-G400 platform (MGI Tech Co., Ltd., Shenzhen, China). This process generated raw sequencing data as short reads, representing the DNA fragments.

Variant Classification and Analysis: The raw sequencing data (FASTQ files) were uploaded to the SEQ Platform (Genomize Inc., İstanbul, Türkiye). The reads were aligned to the human reference genome GRCh37 using the Burrows-Wheeler Aligner (10). Variant calling was performed using FreeBayes (11), followed by additional steps such as Polymerase Chain Reaction (PCR) deduplication and indel realignment using Genomize's proprietary algorithms. Identified variants were annotated using VEP v102 (12) to provide functional annotations. American College of Medical Genetics (ACMG) pathogenicity classification was employed, using Genomize's proprietary algorithm, based on the guideline published by Richards et al. (13).

CNV Analysis: CNV analysis was conducted using the SEQ Platform from Genomize Inc. Reads aligned to the human reference genome GRCh37 were processed with the GATK gCNV tool v4.1.8.1 (14), using optimized parameters to detect and analyze CNVs. Additional information from external sources, such as ClinVar entries, bioinformatics-based effect prediction tool scores, and variant frequency values in the SEQ cohort, were considered during the analysis to assess variant significance and frequency further.

PCR: Long-range PCR was performed using LongAmp® Taq 2X Master Mix (M0287L, New England Biolabs, NEB) following the manufacturer's protocol. The reaction mixture was prepared in a final volume of 25 µL, containing 13.0 µL LongAmp® Taq 2X Master Mix, 1.0 µL 50 mM $MgCl_2$, 1.0 µL forward primer (*B3GLCT*-LONG-Y15F: CAACCTCAGCACTTTGGGAG), 1.0 µL reverse primer (*B3GLCT*-LONG-Y15R: CCCCGGTATCAGTAGAAGGC), 5.0 µL nuclease-free water (ddH_2O), and 80 ng genomic DNA. Thermal cycling conditions included an initial denaturation at 95 °C for 5 minutes, followed by 35 cycles of 94 °C for 30 seconds (denaturation), 60 °C for 1 minute (annealing), and 65 °C for 3 minutes (extension), with a final extension at 65 °C for 10 minutes and an indefinite hold at 4 °C. PCR products were analyzed by agarose gel electrophoresis and visualized under UV light.

Statistical Analysis

Data analysis was performed using the Statistical Package for the Social Sciences (SPSS) version 23.0 for Windows (SPSS, Inc., Chicago, IL). Descriptive statistics for quantitative data are presented as arithmetic mean, SD, median, and minimum-maximum values.

Results

Clinical Findings

Eleven patients (seven male, four female) from six families with a mean age at diagnosis of 11.1 ± 12.5 years were included. Five families had first- and/or second-degree consanguineous marriages, and all the families included in the study originated from the same village. Four family pedigrees (F3, F4, F5, F6) were remarkable due to the presence of multiple affected individuals, and five pedigrees (F1, F2, F3, F4, F6) were noteworthy in terms of recurrent abortus and intrauterine termination due to multiple congenital abnormalities, including cleft lip and/-or palate and hydrocephaly (Table 1, Supplementary Data 1). All patients were referred to our department due to short stature, facial dysmorphism, and severe brachydactyly. Except for patients 7, 8, 10, and 11, all others exhibited "happy" facial appearance and muscular body build. The median age at admission was 2.74 years, ranging from 2 months to 41 years. The mean SDS for height and weight at admission were -4.4 ± 0.9 and -3.8 ± 1.8, respectively. The median age at the last evaluation was 5.4 years, with ages ranging from 0.8 to 42 years. At this evaluation, the mean SDS of height, weight, and head circumference were -4.1 ± 1.1, -3.1 ± 1.1, -1.9 ± 0.9, respectively. On first examination, all patients displayed similar facial gestalt (Figure 1a-k). Three patients (P5, P8 and P9) had cleft lip/palate, which was operated on during infancy (Figures 1e, g, j). Interestingly, P9 displayed gingival hypertrophy on the upper incisors (Figure 1n). Echocardiography and abdominal ultrasonography were performed in all patients except P11, who had severe joint contractures and intellectual disability, which prevented us from conducting a comprehensive evaluation. Six patients (P3, P5, P6, P7, P9 and P10) exhibited genitourinary abnormalities, including an anterior-placed anus, deep sacral dimple, and bilateral cryptorchidism. Urinary ultrasonography revealed a duplex collecting system in the left kidney of P10, who subsequently underwent surgery for nephrolithiasis. A skeletal survey was performed in all cases, which revealed no significant findings

Table 1. Demographic, clinical, and radiological features of the patients in the present study

Family	**1**	**2**	**3**		4				**5**	**6**	
Patient No	**1**	**2**	**3**	**4**	**5**	**6**	**7**	**8**	**9**	**10**	**11**
Consanguinity	Same village	First cousin	Second cousin	First cousin	First cousin	First cousin	First cousin	First cousin	Second cousin	First cousin	
Sex	M	M	F	F	M	M	F	M	M	F	M
Gestational age (weeks)	32	Full term	32	35	39	Full term	36	N/A	35	38	N/A
Birth weight (g/SDS)	1750/-0.0	2300/-2.6	1530/-0.7	1750/-1.7	2390/-2.9	2200/-2.9	1850/-2.6	N/A	1300/-4.0	3200/-0.1	N/A
Birth length (cm/SDS)	43/-0.0	N/A	42/-0.2	44/-0.8	47/-1.6	46/-1.7	40/-3.1	N/A	43/-1.45	49/-3.0	N/A
IUGR	-	+	+	+	+	+	-	N/A	+	N/A	N/A
Antenatal US	Short extremities at third trimester	Short extremities at third trimester	IUGR	Short extremities at third trimester	IUGR	Short extremities at third trimester	Short extremities at third trimester, macrocephaly	N/A	Hydrocephaly	N/A	N/A
Oligo/polyhydramnios	-/-	-/+	-/-	-/+	-/-	-/-	-/-	N/A	-/-	N/A	N/A
Neonatal ICU requirement	Respiratory distress	-	Respiratory distress	Respiratory distress	Feeding difficulties, cleft lip/palate	Respiratory distress	Respiratory distress	-	Respiratory distress, feeding difficulties, cleft lip/palate, hydrocephalus	-	-
Family history	Recurrent abortus										
Age at admission (years)	$1^{4/12}$	$10^{5/12}$	$5^{4/12}$	$0^{2/12}$	$1^{7/12}$	$2^{8/12}$	$0^{2/12}$	$41^{5/12}$	$0^{6/12}$	$15^{3/12}$	$26^{3/12}$
Height at admission (cm/SDS)	64.5/-4.9	115/-4.1	94/-3.7	47/-4.8	72.5/-3.2	77/-4.6	48.3/-3.9	145.3/-5.0	51/-6.5	141/-3.4	150/-4.2
Weight at admission (kg/SDS)	7.4/-3.3	19.7/-3.5	12.5/-3.1	2.9/-3.9	7.6/-3.6	6.9/-7.1	4/-1.8	59.5/-1.4	2.3/-7.3	37/-3.5	46/-3.5
OFC at admission (cm/SDS)	N/A	50.5/-2.2	N/A	N/A	46/-1.7	47.5/-1.5	39/-0.1	56/-1.1	N/A	53/-2.0	55/-1.8
Age at diagnosis (years)	$3^{4/12}$	$10^{7/12}$	$9^{1/12}$	$5^{5/12}$	$2^{9/12}$	$2^{10/12}$	$0^{9/12}$	$41^{5/12}$	$4^{3/12}$	$15^{9/12}$	$26^{10/12}$
Current age (years)	$3^{8/12}$	$12^{0/12}$	$10^{1/12}$	$5^{5/12}$	$3^{2/12}$	$3^{7/12}$	$0^{9/12}$	$41^{5/12}$	$4^{9/12}$	$15^{9/12}$	$26^{10/12}$
Current height (cm/SDS)	82/-4.8	124.1/-3.7	127/-1.8	83.5/-6.0	85/-3.3	85/-3.9	60/-4.4	145.3/-5.0	90/-4.3	141.7/-3.5	150/-4.5
Current weight (kg/SDS)	11.0/-3.3	28.1/-2.2	27.5/-1.0	10.3/-4.7	10.1/-3.6	10.0/-4.1	6.0/-3.0	59.5/-1.4	11.7/-3.7	37.7/-3.4	46.0/-3.5
Current OFC (cm/SDS)	47/-2.6	52/-1.8	51/-1.3	47/-2.7	47/-2.2	47/-2.5	45/0.1	56/-1.1	48/-2.4	53/-2.1	55/-1.8
Dysmorphic features											
Round face	+	+	-	+	+	+	+	+	-	+	+
Long face	-	-	+	-	-	-	-	-	+	+	-
Prominent forehead	+	-	+	+	+	+	+	-	+	-	-
High anterior hairline	+	-	+	+	+	+	+	+	+	+	+

Table 1. Continued

Widows peak	+	+	-	-	+	+	-	-	-	+	-
Hypertelorism	+	+	+	+	+	+	+	+	+	+	+
Upslanting palpebral fissures	-	+	+	+	+	+	+	+	+	-	-
Long philtrum	+	+	+	+	+	+	+	+	+	+	+ (tented)
Cupid bow upper lip	+	+	+	+	+	+	+	+	+	+	+
Thin upper vermillion	+	+	+	+	+	+	+	+	+	+	+
Cleft lip/palate	-	-	-	-	+ / +	-	-	+ /-	+ / +	-	-
Widely spaced teeth	+	-	-	-	-	-	-	-	+	-	+
Gingival hypertrophy	-	-	-	-	-	-	-	-	+	-	-
Short neck	+	+	+	+	+	+	+	+	+	+	+
Low set ears	+	+	-	+	+	+	+	-	+	+	+
Preauricular pit/cyst	-	-	-	-	-	+	+ Unilateral	-	+	-	-
Double whorl	-	-	-	-	-	+	-	-	-	-	-
Single palmar crease	-	-	+	-	-	+	+	-	+	+	-
Hearing loss	-	-	-	-	-	-	-	-	-	-	N/A
Ocular defects											
Peters anomaly	-	+	-	+	-	+	-	+	+	+	+
Anterior chamber anomaly	-	+	-	+	-	+	-	+	+	+	+
Cataract	+	-	-	Bilateral	-	-	+	-	+ Left	-	N/A
Iris atrophy	-	-	-	+	-	-	-	-	+	-	N/A
Retinal atrophy	+	-	+	+	+	+	-	+	-	-	-
Glaucoma	-	+	-	-	-	-	-	+	+	-	N/A
Iris coloboma	-	-	-	+	-	+	-	-	-	-	-
Retinal coloboma	-	-	-	+	-	+	-	-	-	-	N/A
Optic disc	Pale	-	Pale	-	Pale	-	-	Pale	-	-	N/A
Cardiac defects											
ASD	-	+	-	-	-	-	+	-	+	-	N/A
VSD	-	-	-	-	-	-	-	-	+	-	N/A
Pulmonary stenosis	-	-	-	-	-	-	+	-	-	-	N/A
Bicuspid aorta	-	+	-	-	-	-	-	-	-	-	N/A
PFO	-	-	-	-	+	-	-	-	-	-	N/A
Genitourinary abnormalities											
Hydronephrosis	-	-	-	-	-	-	-	-	-	-	N/A
Renal duplication	-	-	-	-	-	-	-	-	-	+	N/A
Cryptorchidism	-	-	-	-	Bilateral	Bilateral	-	-	Bilateral	-	-
Inguinal hernia	-	-	-	-	-	-	-	-	+	-	-
Hypoplastic clitoris/ labia majora	-	-	-	-	-	-	-	-	-	-	-
Nephrolithiasis	-	-	-	-	-	-	-	-	-	+	-
Anterior placed anus	-	-	+	-	-	-	+	-	+	-	-
Sacral dimple	-	-	+	-	-	-	-	-	+	-	-

Table 1. Continued

Skeletal findings																									
Rhizomelic shortening	+		-	+		+		+		+		+			+			+							
Brachydactyly	+	+		+	+		+	+		+		+			+			+							
Broad hands/feet	+	+		+		+		+		+		+			+			+							
Fifth finger clinodactyly	+		-	+		+		+		-		-			+			+							
Vertebral defects	-		-	-		-		-		-		-			-			-							
Neurologic impairment																									
DD/ID	+		-	-	+	+		+		-		+ (mild)			+			+							
ADHD	-		-	+	+	-		-		-		-			-			-							
CC hypoplasia/ agenesis	-		-	-	?	-		-		+		-			+			-		N/A					
Enlarged ventricules/ hydrocephaly	-		-	-	-	-		-		+		-			+			-		N/A					
Tip toe walking	+	+		-	-	-		-		-		-			+			-		Wheelchair-bound					
Feeding difficulties	-	-		+	+	-		-		-		-			+			-		-					
Other	Sludge in the gallbladder	GH treatment	-	-	-	-		-	Epilepsy		Partial hypergonadotropic hypogonadism	-						-		-					

ADHD: attention deficit hyperactivity disorder, ASD: atrial septal defect, CC: corpus callosum, DD: developmental delay, F: female, GH: growth hormone, ICU: intensive care unit, ID: intellectual disability, IUGR: intrauterine growth retardation, M: male, N/A: not available, PFO: patent foramen ovale, SD: standard deviation, USG: ultrasonography, VSD: ventricular septal defect SDS: standard deviation score, US: ultrasonography, N/A: not applicable

of skeletal dysplasia apart from severe brachydactyly. P2 was diagnosed with growth hormone deficiency based on provocative GH tests (clonidine and L-dopa stimulation) and has been receiving growth hormone treatment for one year, leading to a height increase of 9.5 cm during this period. The Turkish version of the Denver Developmental Screening Test was used for patients under five years old, while the Porteus Maze Test and Kent EGY test assessed performance and verbal IQ in older patients. Five individuals (P1, P4, P5, P6, P7) exhibited mild developmental delays across fine motor, gross motor, personal-social, and language skills. In contrast, P9 demonstrated a profound global developmental delay in all domains. In addition, P4 exhibited attention deficit hyperactivity disorder (ADHD) requiring medical treatment. P2 and P3 exhibited normal intelligence, yet P3 presented with ADHD. P10 showed mild intellectual disability, while her brother, P11, was compatible with severe intellectual disability. Moreover, P7 had experienced afebrile seizures from three months of age. Cranial magnetic resonance imaging (MRI) revealed a thin corpus callosum and hydrocephalus in both P7 and P9 (Figures 2a, b). P9 required a ventriculoperitoneal shunt during the neonatal period. P8, the oldest patient in the cohort, had mild hepatosteatosis and lobulation in the right kidney. Cranial tomography showed enlargement of the third and lateral ventricles, along with atrophy of the hemispheric sulci and fissures. In addition, a diffuse decrease in the density of the periventricular white matter was noted, which was evaluated as being consistent with chronic ischemic changes (Figures 2c, d). He exhibited mild intellectual disability, as he was unable to learn to read or perform simple mathematical calculations. Moreover, he had been married for six years without having children, suggesting infertility. Elevated follicle-stimulating hormone (FSH) (13.76 mIU/mL) and luteinizing hormone (LH) (10.0 mIU/mL) levels were detected, along with low testosterone (1.59 ng/mL) and anti-Müllerian hormone (1.60 ng/mL). These findings suggest partial hypergonadotropic hypogonadism. Unfortunately, a spermiogram could not be performed to assess sperm parameters.

Ophtalmologic Findings

P10 had bilateral central corneal haze with mild to moderate decreased visual acuity and was considered to be mild (Figure 3a). P4 had central corneal leucoma covering the pupil and anterior synechiae in the left eye and iris, and retinal coloboma in the right eye (Figure 3b). The right eye had cataract surgery and was pseudophakic. P6 displayed right corneal leucoma, prominent iris papillae, and iris and retinal coloboma in the same eye (Figure 3c). Both P4 and P6 were classified as having a moderate form. P2 and

Figure 1. Photographs of older patients in the study. **a)** P2 (11 years and 8 months), **b)** P3 (10 years), **c)** P10 (15 years and 9 months), **d)** P11 (26 years), and **e)** P8 (41 years). Common dysmorphic features include hypertelorism, a high anterior hairline, a thin vermillion border with a Cupid's bow-shaped upper lip, and a long philtrum. Additionally, P2, P10 and P11 displayed low-set ears **(a, c, d)**, while P3 exhibited up-slanting palpebral fissures **(b)**. Second row: Photographs of patients under six years old. **f)** P1 (3 years and 8 months), **g)** P5 (3 years and 2 months), **h)** P4 (5 years and 5 months), **i)** P6 (3 years and 7 months), **j)** P9 (4 years and 9 months), and P7 (2 months). All patients exhibit nearly identical facial features, including hypertelorism, a long philtrum, low-set ears, and a thin vermillion border. Note the short neck and muscular body build, which overlap with features of geleophysic dysplasia. Hands are notably short with brachydactyly. P5 and P9 had cleft lip/palate repair surgery **(g, j)**. Third row: Characteristic findings of PTRPLS in the present study. P4 had corneal clouding in the left eye **(l)**. P9 exhibited severe glaucoma in the left eye, resulting in vision loss, and underwent surgeries for both glaucoma and cleft lip/palate **(m)**. Additionally, P9 displayed remarkable gingival hypertrophy, an uncommon feature of PTRPLS **(n)**. P6 had an ear pit and low-set, posteriorly rotated ears **(o)**

PTRPLS: Peters-Plus syndrome

P9 had unilateral corneal leucoma with severe visual loss, corneo-lenticular adhesion, and glaucoma (Figure 3d). P9 underwent diode laser treatment twice for glaucoma and is currently on topical latanoprost and dorzolamide-timolol as part of the treatment regimen. P10 and P11, who are siblings, presented with bilateral corneal involvement. However, P11 had more severe involvement in the left eye, leading to vision loss. P1 and P7 exhibited posterior subcapsular opacification, which caused mild visual impairment. P1, P3, and P5 exhibited no corneal opacity but presented with a pale optic disc and chorioretinal atrophy. Moreover, P1 was diagnosed with crystalline fibrils in the vitreous. P8 had mild corneal haze in one eye, high myopia (-20 diopters), and glaucoma in both eyes. He was using travoprost drops bilaterally. P2, P4, and P5 displayed uni–and/ or bilateral microcornea.

Molecular Analysis

P1 had previously undergone karyotype and chromosomal microarray before presenting to our clinic. We conducted a CES due to the presence of syndromic features and family history suggestive of autosomal recessive inheritance. No pathogenic or likely pathogenic variant related to the phenotype could be detected. However, in all patients, CNV detection algorithms identified a 690 bp homozygous deletion in the 13q12.3 region (hg19: chr13:31903374-31904064),

encompassing exon 15 of *B3GLCT* (NM_194318.4) (Figure 4a, c). There were no other morbid OMIM genes except for *B3GLCT* in the deleted region on chromosome 13q12.3. This alteration was found to be haploinsufficient by Franklin. However, the ClinGen database did not provide reliable data about the haploinsufficiency (HI) score. According to the ACMG criteria, the pathogenicity of this CNV alteration is uncertain and has not been reported in public databases, including Database of Genomic Variants and GnomAD. Analysis of BAM files using the Integrative Genomics Viewer

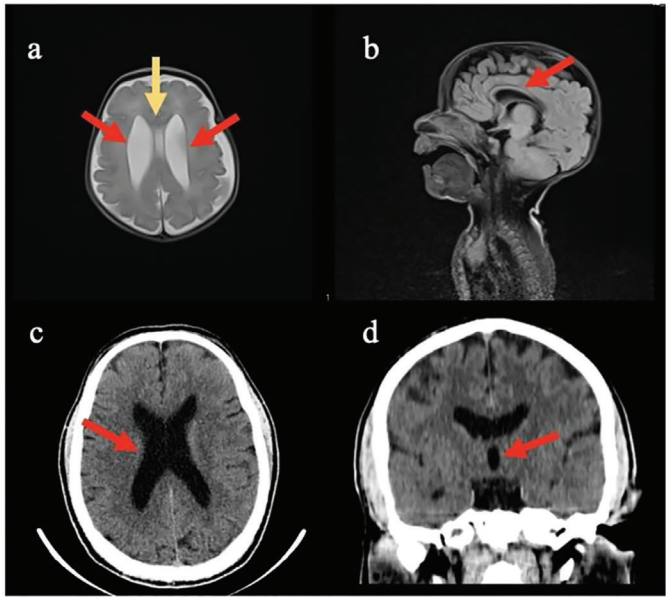

Figure 2. MRI findings of Patient 7. Widened lateral ventricles (indicated by red arrows) and a cavum septum pellucidum vergae variant (highlighted by a yellow arrow) were observed **(a)**. Corpus callosum hypoplasia (red arrow) was seen in the sagittal section **(b)**. CT imaging of Patient 8. The ventricular system and sulci appeared widened (red arrows), indicating cerebral atrophy **(c, d)**. Additionally, a diffuse decrease in periventricular white matter density was observed, consistent with chronic ischemic changes **(d)**

MRI: magnetic resonance imaging, CT: computed tomography

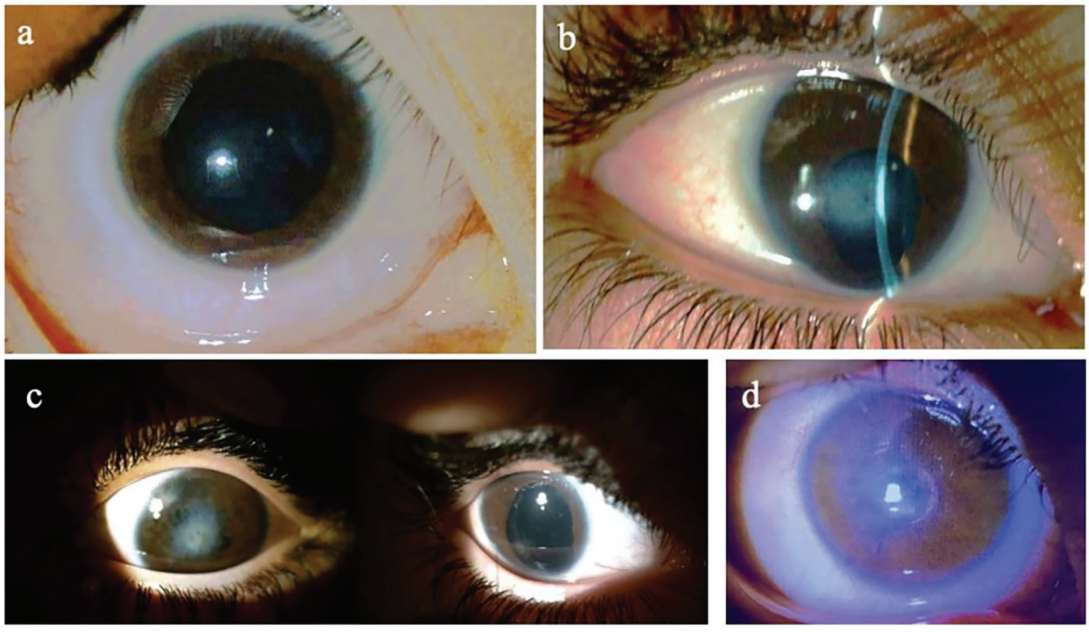

Figure 3. Ophthalmologic abnormalities detected in the study **a)** Patient 10; corneal haze, **b)** Patient 4; central corneal leucoma covering the pupil and anterior synechiae (left photo) and iris coloboma and pseudophakic (right photo). **c)** Patient 6; central corneal leucoma and iris coloboma. **d)** Patient 2; central and nasal paracentral corneal leucoma with corneo-lenticular adhesion

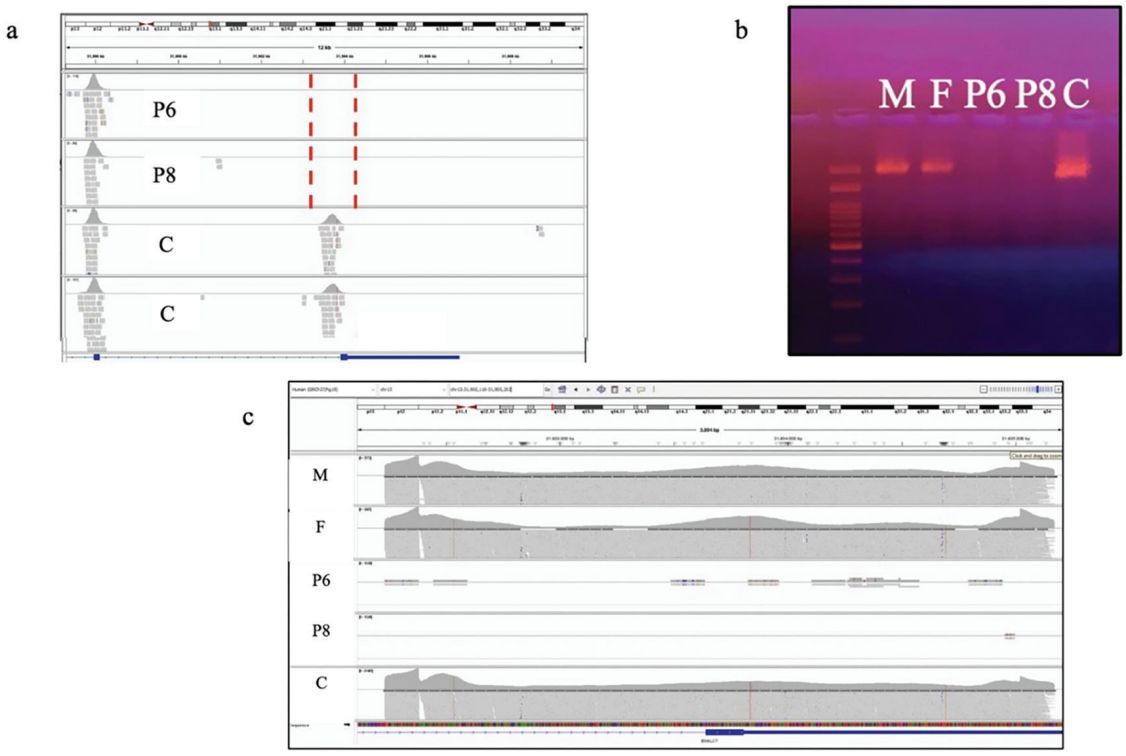

Figure 4. NGS-based CNV analysis. **a)** CNV alteration of the two probands on the IGV vizulation. While controls demonstrated no alteration of CNV, the first and second rows show the O copy number of the 15th exons of the *B3GLCT* gene. **b)** Given that the parents are known to be first cousins and predicted to be obligatory heterozygous carriers of the deletion, the detected amplicons in their PCR reactions are likely derived from their non-deleted, healthy alleles. This assumption is supported by the fact that the healthy control, possessing two non-deleted alleles, also showed similar amplification. **c)** NGS-based CNV analysis through CES revealed a decreased read depth in the parental samples, indicative of a potential heterozygous deletion

C: control, F: father, M: mother, P6: patient 6, P8: patient 8, NGS: Next-Generation Sequencing, CNV: copy number variation, IGV: Integrative Genomics Viewer, CES: clinical exome sequencing

(IGV) revealed zero read depth at exon 15 of *B3GLCT*, despite adequate read depth in control samples sequenced within the same run. Confirmation analysis was planned but no specific MLPA probe for *B3GLCT* was available. Chromosomal microarray analysis had previously failed to identify the deletion. Long-range PCR was considered for confirmation. The nearest exons with sufficient read depth upstream and downstream of exon 15 of *B3GLCT* were exon 14 of *B3GLCT* and exon 1 of *RXFP2*, respectively. Since the exact breakpoints could not be predicted, two long-range PCR reactions using different primer pairs were conducted. NGS-based CNV analysis revealed a decreased read depth in the parents, which indicates a reduced number of sequencing reads aligning with the region of interest. This suggests that the parents are heterozygous carriers of the deletion, as the decreased read depth corresponds to a loss of one copy of the affected genomic region. To demonstrate the carrier status of the patients, primers were designed for the region of interest. We used control, maternal, paternal, and patient samples. The observed PCR amplification in the parents and healthy control indicates the presence of at least one intact allele containing the primer-binding sites, leading to successful amplification. In contrast, no amplification in the patients suggests a homozygous deletion of the target region (Figure 4b).

Discussion

Over the past decade, employing NGS analysis to uncover inherited disorders has significantly expanded our understanding of the genetic basis of Mendelian disorders. NGS enables analysis of multiple regions of the genome in a single reaction and has proven to be both cost-effective and clinically effective for the investigation of patients with genetic conditions (15). Unfortunately, it has limitations in its ability to detect CNVs, such as single or multiple exon deletions, which are known to be important contributors to genetic disorders. The application of CNV detection

algorithms in NGS diagnostic services may facilitate immediate improvements in the clinical care of individuals with heterogeneous Mendelian disorders (16,17). P1, the proband of our study, presented with disproportionate short stature and facial dysmorphism and was evaluated for a possible genetic condition. However, despite extensive molecular analyses, including karyotype, microarray, and targeted gene panels, a definitive diagnosis could not be established. Subsequently, ten additional patients, all presenting with nearly identical symptoms, visited our clinic, albeit with varying degrees of clinical severity. NGS-based CNV analysis was subsequently employed to identify significant CNVs that could potentially explain the genetic basis of the condition. All patients were found to harbor a 690 bp homozygous deletion in the 13q12.3 region, covering the fifteenth exon of the *B3GLCT* gene. The consistent homozygous deletion in exon 15 of the *B3GLCT* gene across all unrelated patients likely results from a founder effect, as they originate from the same village, indicating a shared common ancestor. This group represents the first report of a homozygous which is also the smallest exonic deletion in the 13q12.3 region, only encompassing the *B3GLCT* gene. Other reports have shown that CNV alterations in the same region are causative for PTRPLS, with gene-targeted deletion/duplication analysis identifying four individuals with PTRPLS in the published literature (1,18,19). The first deletion was identified by Lesnik Oberstein et al. (1) using array-based comparative genomic hybridization, revealing a 1.5 Mb interstitial deletion in the 13q12 region of chromosome 13, containing the *B3GLCT* gene, along with the common c.660 + 1G > A variant on the other allele in two siblings. Similarly, Haldeman-Englert et al. (19) reported a heterozygous 781 kb deletion alongside the common c.660 + 1G > A variant in a male patient with typical PTRPLS features. Comparison of the deletion identified in our study with previous reports reveals a common overlapping region confined to the smallest area of 13q12.3, which includes exon 15 of the *B3GLCT* gene. Furthermore, while the other two reports documented heterozygous deletions encompassing multiple morbid OMIM genes, this deletion is particularly significant as it is homozygous and represents the smallest deletion reported to date, affecting only the *B3GLCT* gene. In the literature, documented pathogenic alleles consist of 86% splicing mutations, 6% truncating mutations, 4% missense mutations, and 4% whole gene deletions (7). Therefore, based on our findings and previous studies, we believe that NGS-based CNV analysis can play an important role in the diagnosis of genetic variations, including small deletions and duplications associated with inherited Mendelian disorders.

TSRs are present in over 60 human proteins but only 49 of these have the required consensus sequence for fucosylation and subsequent modification by *B3GLCT*, including secreted matrix proteins like thrombospondin 1 (TSP1) and TSP2, as well as all members of the ADAMTS and ADAMTSL families (20). Previous studies have demonstrated that HI of ADAMTS9 and ADAMTS20 is responsible for anterior segment dysgenesis and cardiac anomalies in animal models (21,22,23). Moreover, both ADAMTS9 and ADAMTS20 play a role in palatal closure, which is the definitive mechanism underlying the observed cleft palate phenotype (21). Furthermore, ADAMTS20-null mice exhibit a white spotting defect and a high degree of hydrocephalus (24). Mouse *B3GLCT* knockout models exhibit craniofacial and skeletal abnormalities similar to those observed in PTRPLS patients (24). These independent observations collectively suggest that PTRPLS specifically results from secretion defects in certain target proteins of *B3GLCT* (25). In addition, loss of *B3GLCT* significantly reduces the secretion of ADAMTSL2 (25). Geleophysic dysplasia (GD), caused by mutations in *ADAMTSL2* leading to reduced secretion of the mutant protein compared to the wild-type protein, shares several common symptoms with PTRPLS (25,26). In our cohort, P1, P2, P3, and P5 were initially diagnosed with GD based on severe brachydactyly, muscular body build, and a characteristic “happy” facial appearance. However, severe cardiac involvement in GD and distinct ocular findings in PTRPLS may provide valuable clinical clues for distinguishing between the two phenotypes. Consequently, comprehensive evaluation of both systems is essential, and we recommend considering PTRPLS in individuals who test negative for GD mutations.

Affected individuals present with similar phenotypes and complaints, yet there is significant intra- and inter-familial variability (1,19). In the present study, we noted phenotypic variability consistent with previous reports on PTRPLS. The study by Lesnik Oberstein et al. (1) highlighted that even within a genetically homogeneous group (homozygous for c.1020-1G > A), cognitive outcomes ranged from normal secondary education to severe cognitive impairment, suggesting the influence of additional genetic or environmental modifiers. Similarly, Haldeman-Englert et al. (19) proposed that the variable phenotypes in patients with deletions involving *B3GLCT* may result from the multisystemic effects of glycosylation defects or the involvement of other genes within the deleted region. Furthermore, no clear genotype-phenotype correlation has been established to date, and the cause of intra- and inter-familial variability remains unknown. It is likely that factors beyond the primary genetic variant, such as modifier genes, epigenetic influences, or environmental factors, contribute to the phenotypic heterogeneity observed in PTRPLS. Ophthalmological anomalies, which can provide clues for

an accurate diagnosis, have emerged as another feature that demonstrates this variability in this study. Four patients (P1, P3, P5, and P7) did not exhibit anterior segment dysgenesis or Peters anomaly. However, three of the four presented with retinal atrophy, except for P7. Ocular involvement is generally bilateral but unilateral cases have also been reported (27). Consistent with the literature, Peters anomaly was observed bilaterally in five of our patients and unilaterally in two. Cataract and glaucoma, common features that can also occur later in life, were observed in six of 11 patients in our cohort. Interestingly, unusual eye symptoms, including severe myopia, iris coloboma, retinal coloboma, optic atrophy, and microcornea, were noted in nine patients. Cardiac involvement is another systemic feature that varies among affected individuals. Congenital heart defects occur in approximately 30% of cases (1). Consistent with the literature, we observed bicuspid aorta, atrial septal defect, ventricular septal defect, patent foramen ovale, and pulmonary stenosis in 4 of 11 patients (36%).

Despite severe short stature, the skeletal survey showed no definitive evidence of skeletal dysplasia, apart from brachydactyly. Our observations suggest that brachydactyly was more pronounced in patients under five years of age than in older individuals. In the context of PTPRLS, GH therapy has been shown to yield positive results in a limited number of cases. Three reports in the literature have described patients with PTRPLS who demonstrated a good response to GH therapy. In these cases, GH deficiency was identified, which may have contributed to the patients' short stature. However, in all three studies, the molecular diagnoses of the patients were not established; instead, the diagnosis of PTRPLS was based on clinical findings. One of these reports also highlighted that pituitary dysfunction is well known to be associated with midline defects, encompassing a broad spectrum of congenital midline anomalies. These range from severe, nonviable conditions to milder presentations, such as isolated cleft lip or palate, as observed in PTRPLS. Notably, the prevalence of GH deficiency is reported to be 40 times higher in children with cleft lip and palate or isolated cleft palate compared to those without such anomalies. This strong correlation between pituitary dysfunction and congenital craniofacial malformations suggests that every child with midline facial defects should undergo a pituitary evaluation (2,28,29). Another study reported two siblings diagnosed with PTRPLS who also had GH deficiency and a small pituitary gland, yet no variants were detected in the *B3GLCT* gene (29). This reinforces the importance of performing cranial MRI in patients with GH deficiency and underscores the need to investigate CNVs in cases negative for *B3GLCT* variants. In our cohort, only P2 exhibited GH deficiency. Treatment with recombinant GH resulted in an increased growth velocity (9.5 cm/year), improving height from -4.0 to -3.3 SDS over one year of therapy, indicating a promising outcome. Interestingly, he had no clefting, and cranial MRI revealed no abnormalities. However, as demonstrated by previous reports of GH deficiency in children with PTRPLS, a pituitary evaluation should be considered, particularly in the presence of midline facial defects, and the growth hormone/insulin-like growth factor axis should be assessed. Further studies with larger cohorts are needed to better understand the prevalence of GH deficiency in PTRPLS, the long-term benefits of GH therapy, and its potential role in managing growth impairments in this population.

In our cohort, four patients were over the age of 10, and only one of them, P8 (40 years old), was diagnosed with partial hypergonadotropic hypogonadism. This diagnosis was based on elevated gonadotropin levels (FSH and LH) alongside low testosterone and anti-Müllerian hormone levels. To the best of our knowledge, hypergonadotropic hypogonadism has not been previously reported in patients with PTRPLS. This raises the question of whether it represents an unrecognized feature of the syndrome or an unrelated coexisting condition. Further studies involving additional patients are needed to clarify this association. However, we recommend monitoring patients for hypogonadism as they age.

Study Limitations

A limitation of the study is the inability to determine the exact breakpoints of the suspected deletion using an alternative method. However, the amplification failure of LR-PCR indirectly indicated the deletion. Furthermore, the suspected deletion was identified in all patients and their parents through NGS-based CNV analysis.

Conclusion

Previous studies have demonstrated that CNVs can contribute to the pathogenesis of PTRPLS. Deletions involving the *B3GLCT* gene can result in a clinical phenotype similar to that caused by point mutations within the gene. The findings reported herein highlight the importance of CNVs, especially in cases where standard genetic testing fails to detect small deletions/duplications. The accurate detection of CNVs using NGS-based CNV analysis highlights its value as a powerful tool in genetic diagnostics. Consequently, our study emphasizes the importance of incorporating NGS-based CNV analysis into routine genetic testing, which may lead to better clinical outcomes and personalized management for individuals with Mendelian disorders.

Ethics

Ethics Committee Approval: The study received approval from the Non-invasive Clinical Research Ethical Committee of University of Health Sciences Türkiye, Diyarbakır Gazi Yaşargil Training and Research Hospital (approval number: 46, date: 10.05.2024).

Informed Consent: Written informed consent was obtained from the parents.

Acknowledgments

We thank our patients and their families for their collaboration and participation, and we are thankful to Aşkın Özel for his technical support.

Footnotes

Authorship Contributions

Concept: Akçahan Akalın, Şervan Özalkak, Ruken Yıldırım, Veysel Öz, Edip Ünal, Leyla Hazar, Tahir Atik, Özgür Çoğulu, Esra Işık, Design: Akçahan Akalın, Enise Avcı Durmuşalioğlu, Esra Işık, Data Collection or Processing: Akçahan Akalın, Leyla Hazar, Türkan Turkut Tan, Yusuf Can Doğan, Tahir Atik, Özgür Çoğulu, Esra Işık, Analysis or Interpretation: Enise Avcı Durmuşalioğlu, Esra Işık, Literature Search: Akçahan Akalın, Şervan Özalkak, Ruken Yıldırım, Veysel Öz, Edip Ünal, Leyla Hazar, Esra Işık, Writing: Akçahan Akalın, Leyla Hazar, Esra Işık.

Financial Disclosure: The authors declare that no funds, grants, or other support were received during the preparation of this manuscript.

References

1. Lesnik Oberstein SA, Kriek M, White SJ, Kalf ME, Szuhai K, den Dunnen JT, Breuning MH, Hennekam RC. Peters Plus syndrome is caused by mutations in B3GALTL, a putative glycosyltransferase. Am J Hum Genet. 2006;79:562-566.
2. Maillette de Buy Wenniger-Prick LJ, Hennekam RC. The Peters' plus yndrome: a review. Ann Genet. 2002;45:97-103.
3. Shah PR, Chauhan B, Chu CT, Kofler J, Nischal KK. Ocular phenotype of Peters-Plus syndrome. Cornea. 2022;41:219-223.
4. Zaidman GW, Flanagan JK, Furey CC. Long-term visual prognosis in children after corneal transplant surgery for Peters anomaly type I. Am J Ophthalmol. 2007;144:104-108.
5. Bhandari R, Ferri S, Whittaker B, Liu M, Lazzaro DR. Peters anomaly: review of the literature. Cornea. 2011;30:939-944.
6. van Schooneveld MJ, Delleman JW, Beemer FA, Bleeker-Wagemakers EM. Peters'-plus: a new syndrome. Ophthalmic Paediatr Genet. 1984;4:141-145.
7. Weh E, Reis LM, Tyler RC, Bick D, Rhead WJ, Wallace S, McGregor TL, Dills SK, Chao MC, Murray JC, Semina EV. Novel B3GALTL mutations in classic Peters plus syndrome and lack of mutations in a large cohort of patients with similar phenotypes. Clin Genet. 2014;86:142-148. Epub 2013 Sep 17
8. Heinonen TY, Maki M. Peters'-plus syndrome is a congenital disorder of glycosylation caused by a defect in the beta1,3-glucosyltransferase that modifies thrombospondin type 1 repeats. Ann Med. 2009;41:2-10.
9. Royer-Bertrand B, Cisarova K, Niel-Butschi F, Mittaz-Crettol L, Fodstad H, Superti-Furga A. CNV detection from exome sequencing data in routine diagnostics of rare genetic disorders: opportunities and limitations. Genes (Basel). 2021;12:1427.
10. Li H, Durbin R. Fast and accurate short read alignment with Burrows-Wheeler transform. Bioinformatics. 2009;25:1754-1760. Epub 2009 May 18
11. Garrison E, Marth G. Haplotype-based variant detection from short-read sequencing. ArXiv. 2012.
12. McLaren W, Gil L, Hunt SE, Riat HS, Ritchie GR, Thormann A, Flicek P, Cunningham F. The Ensembl Variant Effect Predictor. Genome Biol. 2016;17:122.
13. Richards S, Aziz N, Bale S, Bick D, Das S, Gastier-Foster J, Grody WW, Hegde M, Lyon E, Spector E, Voelkerding K, Rehm HL; ACMG Laboratory Quality Assurance Committee. Standards and guidelines for the interpretation of sequence variants: a joint consensus recommendation of the American College of Medical Genetics and Genomics and the Association for Molecular Pathology. Genet Med. 2015;17:405-424. Epub 2015 Mar 5
14. Babadi M, Fu JM, Lee SK, Smirnov AN, Gauthier LD, Walker M, Benjamin DI, Zhao X, Karczewski KJ, Wong I, Collins RL, Sanchis-Juan A, Brand H, Banks E, Talkowski ME. GATK-gCNV enables the discovery of rare copy number variants from exome sequencing data. Nat Genet. 2023;55:1589-1597. Epub 2023 Aug 21 Erratum in: Nat Genet. 2024;56:553.
15. Jamuar SS, Tan EC. Clinical application of next-generation sequencing for Mendelian diseases. Hum Genomics. 2015;9:10.
16. Ellingford JM, Campbell C, Barton S, Bhaskar S, Gupta S, Taylor RL, Sergouniotis PI, Horn B, Lamb JA, Michaelides M, Webster AR, Newman WG, Panda B, Ramsden SC, Black GC. Validation of copy number variation analysis for next-generation sequencing diagnostics. Eur J Hum Genet. 2017;25:719-724. Epub 2017 Apr 5
17. Atik T, Avci Durmusalioglu E, Isik E, Kose M, Kanmaz S, Aykut A, Durmaz A, Ozkinay F, Cogulu O. Diagnostic yield of exome sequencing-based copy number variation analysis in Mendelian disorders: a clinical application. BMC Med Genomics. 2024;17:239.
18. Kapoor S, Mukherjee SB, Arora R, Shroff D. Peters plus syndrome. Indian J Pediatr. 2008;75:635-637. Epub 2008 Aug 31
19. Haldeman-Englert CR, Naeem T, Geiger EA, Warnock A, Feret H, Ciano M, Davidson SL, Deardorff MA, Zackai EH, Shaikh TH. A 781-kb deletion of 13q12.3 in a patient with Peters plus syndrome. Am J Med Genet A. 2009;149:1842-1845.
20. Du J, Takeuchi H, Leonhard-Melief C, Shroyer KR, Dlugosz M, Haltiwanger RS, Holdener BC. O-fucosylation of thrombospondin type 1 repeats restricts epithelial to mesenchymal transition (EMT) and maintains epiblast pluripotency during mouse gastrulation. Dev Biol. 2010;346(1):25-38. Epub 2010 Jul 14
21. Enomoto H, Nelson CM, Somerville RP, Mielke K, Dixon LJ, Powell K, Apte SS. Cooperation of two ADAMTS metalloproteases in closure of the mouse palate identifies a requirement for versican proteolysis in regulating palatal mesenchyme proliferation. Development. 2010;137(23):4029-4038. Epub 2010 Nov 1
22. Dubail J, Vasudevan D, Wang LW, Earp SE, Jenkins MW, Haltiwanger RS, Apte SS. Impaired ADAMTS9 secretion: a potential mechanism for eye defects in Peters plus syndrome. Sci Rep. 2016;6:33974.
23. Kern CB, Wessels A, McGarity J, Dixon LJ, Alston E, Argraves WS, Geeting D, Nelson CM, Menick DR, Apte SS. Reduced versican cleavage

due to Adamts9 haploinsufficiency is associated with cardiac and aortic anomalies. Matrix Biol. 2010;29:304-316. Epub 2010 Jan 22

24. Holdener BC, Percival CJ, Grady RC, Cameron DC, Berardinelli SJ, Zhang A, Neupane S, Takeuchi M, Jimenez-Vega JC, Uddin SMZ, Komatsu DE, Honkanen R, Dubail J, Apte SS, Sato T, Narimatsu H, McClain SA, Haltiwanger RS. ADAMTS9 and ADAMTS20 are differentially affected by loss of B3GLCT in mouse model of Peters plus syndrome. Hum Mol Genet. 2019;28:4053-4066. Erratum in: Hum Mol Genet. 2020;29:2986-2987
25. Vasudevan D, Takeuchi H, Johar SS, Majerus E, Haltiwanger RS. Peters plus syndrome mutations disrupt a noncanonical ER quality-control mechanism. Curr Biol. 2015;25:286-295. Epub 2014 Dec 24
26. Le Goff C, Morice-Picard F, Dagoneau N, Wang LW, Perrot C, Crow YJ, Bauer F, Flori E, Prost-Squarcioni C, Krakow D, Ge G, Greenspan DS, Bonnet D, Le Merrer M, Munnich A, Apte SS, Cormier-Daire V. ADAMTSL2 mutations in geleophysic dysplasia demonstrate a role for ADAMTS-like proteins in TGF-beta bioavailability regulation. Nat Genet. 2008;40:1119-1123.
27. Lesnik Oberstein SAJ, Ruivenkamp CAL, Hennekam RC. Peters Plus Syndrome. In: Adam MP, Feldman J, Mirzaa GM, Pagon RA, Wallace SE, Amemiya A (eds). GeneReviews® [Internet]. Seattle (WA): University of Washington, Seattle; 1993-2025.
28. Lee KW, Lee PD. Growth hormone deficiency (GHD): a new association in Peters' Plus Syndrome (PPS). Am J Med Genet A. 2004;124A:388-391.
29. Al-Gazali L, Shather B, Kaplan W, Algawi K, Ali BR. Anterior segment anomalies of the eye, growth retardation associated with hypoplastic pituitary gland and endocrine abnormalities: Jung syndrome or a new syndrome? Am J Med Genet A. 2009;149:251-256.

Click the link to access Supplementary Data 1: https://d2v96fxpocvxx.cloudfront.net/cf9d60d6-523c-458a-a2e6-78728d3ffbb0/content-images/d9e710fe-1b14-4c32-a139-e11daa146876.pdf